Modification of Azithromycin to Mitigate its Arrest of Autophagy

Authors:

Ryan D Quarrington[1,2], Sylvia A Sapula[3], Susan E Lester[4], Matthew M Miller[5], Vesna Munic Kos[6], Benjamin T Kopp[7,8,9], Hubertus PA Jersmann[1,10], Anton Blencowe [11]*, Eugene Roscioli[1,10,12]*‡.

Affiliations

[1]Adelaide Medical School, University of Adelaide, Adelaide, South Australia, Australia.

[2]Centre for Orthopedic & Trauma Research, Faculty of Health and Medical Sciences, The University of Adelaide, Adelaide, South Australia, Australia.

[3]Health and Biomedical Innovation, UniSA Clinical and Health Sciences, University of South Australia, Adelaide, South Australia, Australia.

[4]Department of Rheumatology, The Queen Elizabeth Hospital, Adelaide, South Australia, Australia.

[5]Department of Premier and Cabinet, Lot Fourteen, Adelaide, South Australia, Australia.

[6]Department of Physiology and Pharmacology, Karolinska Institutet, Stockholm, Sweden.

[7]Center for Microbial Pathogenesis, The Abigail Wexner Research Institute at Nationwide Children's Hospital, Columbus, OH, USA.

[8]Division of Pulmonary Medicine, Nationwide Children's Hospital, Columbus, OH, USA.

[9]Infectious Disease Institute, The Ohio State University, Columbus, OH, USA.

[10]Department of Thoracic Medicine, Royal Adelaide Hospital, Adelaide, South Australia, Australia.

[11]Applied Chemistry and Translational (ACTB) Group, Centre for Pharmaceutical Innovation (CPI), UniSA Clinical and Health Sciences, University of South Australia, Adelaide, South Australia, 5000, Australia.

[12]Centre for Cancer Biology, SA Pathology and University of South Australia, Adelaide, South Australia, Australia.

* Authors contributed equally

‡ Correspondence: Eugene Roscioli
Adelaide Health and Medical Science
Building, Corner of North Terrace and
George St, Adelaide 5005, South
Australia, Australia
Tel +61 8 8313 7088
Email: eugene.roscioli@adelaide.edu.au

Abstract:

Aims/hypothesis: Autophagy plays a critical role in the survival and microbial clearance functions of airway epithelial cells (**AEC**s). Contrary to the known roles of azithromycin (**AZM**) in promoting microbial clearance, our preliminary evidence suggests that AZM inhibits autophagy in mammalian cells – an effect that could potentially promote bacterial residency in chronic respiratory diseases. Here we investigate the structure-activity relationship of AZM *vs* other common macrolides and AZM-3'-*N*-oxide (**AZM-[O]**), to mitigate the off-target arrest of autophagy.

Method: Participant-derived chronic obstructive pulmonary disease (COPD) *vs* control airway biopsies were assessed for intrinsic defects in autophagy gene activity via qRT-PCR array. For *in vitro* studies, the 16HBE14o- AEC line and Western blot were used to assess macrolide *vs* autophagy structure-activity relationships, and autophagic flux by quantifying the protein abundance of LC3B-II *vs* Sequestosome-1. Subsequent assessments of antimicrobial activity were conducted using an *E. coli* model and the micro-broth dilution method. Immunomodulatory outcomes were assessed by quantifying the secretion of IL-6 in a lipopolysaccharide LPS-stimulated THP-1 macrophage model.

Results: Signatures of transcript-abundance showed an overall reduction in autophagy gene activity in COPD *vs* control biopsies. AZM significantly inhibited autophagic flux, evidenced by the accumulation of LC3B-II and Sequestosome-1, compared to its precursors and other macrolides including roxithromycin and clarithromycin. Notably, oxidation of AZM to produce AZM-[O] significantly alleviated this inhibitory effect on autophagy without completely preserving its antimicrobial and immunomodulatory functions.

Conclusion: The potent off-target block of autophagic flux demonstrated by AZM can be negated by manipulation of its ionisation state. We are currently investigating the AZM-protein interactome and further AZM derivatives that preserve the immunomodulatory function of the parent molecule, to provide a new therapeutic option for chronic respiratory disease and to safeguard the efficacy of AZM.

Short title:

Preventing Azithromycin's block of autophagy

Key words:

Airway, Antibiotic, Antibiotic tolerance, Antibiotic Resistance, Autophagy, Azithromycin, Biochemistry, Drug discovery, Epithelial, LC3, Macrolide, Medicinal Chemistry, Off-target effect, Respiratory.

Introduction

The consequences of intracellular bacteria surviving for prolonged periods in individuals who are routinely exposed to our most significant therapeutics captures some of the world's most immediate health priorities: the expansion of bacterial species that simultaneously adapt to exploit the intracellular niche and our frontline antibiotics. Accordingly, a great proportion of the world's population live for years with respiratory conditions that require antibiotic therapy (e.g., cystic fibrosis, chronic obstructive pulmonary disease (**COPD**) and bronchiectasis). For example, despite the broad window to treat COPD, this condition remains in the top three leading causes of mortality (1, 2), and recurrent microbial infection that can reside in long-lived airway epithelial cells (**AECs**) continue to be the primary driver of disease (3-8). Moreover, macroautophagy (hereafter referred to as autophagy), the principal mechanism responsible for clearing intracellular microbes (9), is frequently dysregulated in pulmonary disease (10, 11). Hence, the pulmonary surface in individuals with chronic respiratory disease represent a vast reservoir for bacterial adaptation (12). The convergence of these phenomena coupled with the reliance on antibiotics (to prevent a sudden increase in global mortality (13)), may be the central reason that despite thousands of years of pharmacological innovation (14), current therapeutic options are palliative and airway infections remain central to disease progression. It is critical to safeguard the efficacy of our frontline antibiotics in the absence of therapeutic options that target the causal mechanisms of pulmonary disease.

As for any medical intervention directed against a microbial pathogen, antibiotics can also elicit undesirable off-target effects in mammalian cells. While it is reasonable to justify this when the off-target effects are well tolerated, a greater concern is enhancing biochemical disease mechanisms, that are beyond the sensitivity of diagnostic/clinical inquiry. A prime example of this would be blocking the host-cell's innate bacterial clearance mechanisms. We and others have found that azithromycin (**AZM**) potently blocks autophagy (4, 15, 16). Normally, in the absence of disease, bacteria are encapsulated within autophagosomes and are rapidly eliminated upon lysosomal fusion by digestive enzymes and acidic pH (9). Indeed, the consequences of perturbing the many other autophagy-mediated functions align with remarkable fidelity to the hallmark phenotypes ascribed to pulmonary disease, such as accelerated senescence (17), nutrient deprivation (18), uncontrolled autoimmune-like inflammation (19), dysfunctional cilia (20), and mitochondrial dysfunction (21). The interplay between autophagic dysregulation and respiratory disease is expansive and there have been several attempts to effectively describe their relationship (11, 22-24). One reason this off-target effect by AZM has been left unchecked is because clinical assessments of infection are confined to symptom relief, and methods in diagnostic pathology are not geared to detect intracellular bacteria. Furthermore, to our knowledge autophagy is completely disconnected from clinical and diagnostic inquiry. This points to a scenario whereby AEC are vulnerable to persistent intracellular bacteria while one of their most effective survival mechanisms is inhibited. Hence, it is important to determine how this occurs and whether AZM can be modified to maintain its efficacy and allow the cell's autophagic functions to operate normally.

AZM is a third-generation semisynthetic macrolide and is distinct from its parent molecule erythromycin A (**ERM**), due to expansion of the lactone ring through insertion of a methylated nitrogen atom ((25); and **Fig 2A**). The resulting enhanced pharmacokinetics, spectrum of activity and tolerance of AZM (*vs* ERM) has made it one of the world's most frequently prescribed antibiotics, which also comports with significant stewardship issues (26, 27). In part owing to its lipophilicity, AZM concentrates at the vast surface area afforded by the ciliated airway epithelium and within the airway

surface liquid (25, 28). Coupled with this, AZM's physiochemical properties exhibit a remarkable capacity to passage pH and electrochemical gradients established by cellular and intracellular membranes (29). As lysosomes partition the lowest pH environment in mammalian cells, this makes AZM extremely lysosomotropic. We and others have shown AZM accumulates in lysosomes via non-ionic diffusion at levels orders of magnitude higher than the cytosol or extracellular matrix (30-32). Aside from being sequestered from microbes in the cytosol, AZM increases lysosomal pH via ion trapping due to the protonation of two of its basic functional groups. This prohibits the normal function of lysosomal proteases, blocks autophagosome-lysosome fusion and inhibits autophagic flux with similar efficacy as bafilomycin (a widely applied inhibitor of autophagy) (4, 16). Indeed, a recent systematic review showed that AZM ranked in the bottom four of nineteen antibiotics for efficacy against intracellular *Staphylococcus aureus* (*S. aureus*) in osteomyelitis (33). What is more, the gradual leakage of AZM from lysosomes exposes bacterial communities to sub-lethal amounts of the antibiotic, enhancing their intracellular persistence (5). The importance of addressing this scenario for AZM, autophagy and chronic respiratory disease is further underscored by current concerns surrounding the paucity of new antibiotics entering the drug development pipeline (34, 35).

Given these significant challenges, we assessed the structure-activity relationship (**SAR**) of AZM *vs* autophagy in relation to outcomes of autophagic flux. These outcomes were also compared to other clinically relevant macrolide antibiotics and azithromycin-3'-*N*-oxide (**AZM-[O]**), a partially oxidised AZM derivative designed to counter its protonation in the lysosome. Outcomes for autophagy, inflammation, and bacterial growth were assessed in models of the human airway.

Methods

Clinical sampling and ethics

Ethics approval to perform airway brushings was obtained from the Central Adelaide Local Health Network Human Research Ethics Committee (approval number 12978). Methods were conducted in accordance with the Declaration of Helsinki and with the understanding and the written consent of each participant. Airway brushing was performed by the physicians at the Royal Adelaide Hospital's Department of Thoracic Medicine. Bronchial samples were obtained from consenting control participants with no history of chronic respiratory disease and were never smokers, and inpatient participants with doctor diagnosed and spirometry consistent with COPD (**Table 1**). Human primary bronchial epithelial cells were obtained from the right main bronchi using a catheter brush inserted into a camera guided bronchoscope.

Synthesis of Azithromycin-3'-*N*-Oxide

AZM-[O] was prepared by adapting two previously described methods (36, 37). Azithromycin (100 mg, 134 µmol) was dissolved in methanol (1 mL) in a single necked round bottomed flask (5 mL) and cooled to 0 °C with an ice bath. 30% w/v H_2O_2 (200 µL, 1.96 mmol) was added dropwise over 30 min and the reaction was stirred at 0 °C for 90 min. The mixture was added to ice water (20 mL) and dichloromethane (10 mL) and stirred at 500 rpm for 1 min. A saturated sodium thiosulfate solution (15 mL) was added, and the mixture was transferred to a separating funnel. The organic phase was removed and the aqueous extracted with dichloromethane (2 × 10 mL). The combined organic extracts were dried with magnesium sulfate and filtered under vacuum. The filtrate was concentrated *in vacuo* and dried (0.01 mbar, 22 °C, 16 h) to afford the title compound as a white solid, 86 mg (84%). ESI-MS $[M+H]^+$ calculated = 765.51 m/z;

measured = 765.62 m/z. All reagents were purchased from ChemSupply (SA, Australia) with the exception of azithromycin, which was purchased from Sigma-Aldrich (NSW, Australia).

Cell culture

16HBE14o- (human bronchial airway epithelial cells) were purchased from EMD Millipore Corporation (Temecula, CA, USA), and propagated as per the manufacturers' instructions. Culture flasks were coated with human fibronectin (10 µg/mL), bovine serum albumin (Fraction V Stock, 100 µg/mL), and PureCol (collagen, 30 µg/mL) suspended in α-MEM (each Sigma-Aldrich, MI, USA). 16HBE14o- expansion media was α-MEM (Sigma) supplemented with 10% fetal calf serum, 1× penicillin/streptomycin and 2 mM L-glutamine (GlutaMAX; each Thermo Fisher Scientific, VIC, Australia). Cells were grown in standard mammalian cell culture conditions at 37°C and 5% CO_2, with humidity. Endpoint culture formats were 12-well plates (Corning, NY, USA), seeded with 2×10^5 cells/well in 2 mL of growth media.

The **THP-1** peripheral blood monocyte cell line was purchased from the American Type Culture Collection (Manassas, VA, USA). Growth and differentiation conditions were as previously described (38), with modifications to support conditions that approximate the proteomic profile observed in human macrophages (39). Standard mammalian cell culture conditions were used (37°C and 5% CO2, with humidity), and cells maintained in RPMI 1640 supplemented with 50 µM ß-mercaptoethanol (both Sigma-Aldrich), 10% fetal calf serum, 1× penicillin/streptomycin and 2 mM L-glutamine (as above). Macrophage differentiation was performed for 2×10^5 cells/well (12-well plate format), by supplementing the growth media with 50 ng/mL phorbol-12-myristate-13-acetate (PMA, Sigma-Aldrich) for 16 h, followed by a 48 h rest period.

The cell models were exposed to AZM-[O], solithromycin (**SLM**; Cayman Chemicals, MI, USA), erythromycin A (**ERM**), telithromycin (**TEL**), roxithromycin (**ROX**), clarithromycin (**CLM**; Sigma-Aldrich), erythromycin-9-oxime (**ERM-oxime**) and erythromycin-9,11-imino ether (**ERM-ether**; Toronto Research Chemicals, ON, Canada), dissolved in molecular biology grade dimethyl sulfoxide (DMSO, Sigma-Aldrich) to less than 0.1% v/v in media. Chemical structures of the macrolides were generated using ChemDraw v23.0 (PerkinElmer, MA, USA). Lipopolysaccharide (Sigma-Aldrich) was suspended in ultra-pure water.

Reverse transcription qPCR array analysis

Quantitative reverse transcription real-time PCR (**qRT-PCR**) was performed as previously described (40). Briefly, qRT-PCR was applied to measure transcript abundance in bronchial airway samples. RNA was extracted and genomic DNA eliminated using the RNeasy Plus column system following the manufacturers protocol (QIAGEN, Chadstone, VIC, Australia). RNA was quantified using a NanoDrop One spectrophotometer (Thermo Fischer Scientific). A second gDNA purification was coupled with reverse transcription of RNA (1 µg) into cDNA with the SuperScript IV VILO ezDNase system (Thermo Fischer Scientific) using an Eppendorf Mastercycler (Eppendorf, Hamburg, Germany). cDNA samples were entered into a custom TaqMan low density array (Thermo Fischer Scientific). Sample reaction mixtures were 500 ng cDNA, and TaqMan primer/probes technology in conjunction with TaqMan Fast Advanced Master Mix chemistry (all Thermo Fischer Scientific). The ViiA7 7300 Real Time PCR platform (Applied Biosystems, Carlsbad, California, USA) was used to perform qRT-PCR. Internal reference genes (n=3) to normalize outcomes across the experimental

groups were: *RNA18S5* (Hs99999901_s1), *HMBS* (Hs00609297_m1) and *TBP* (Hs00427620_m1). The complete set of primer/probes are provided in **Supplementary Table S1**.

Western blot

Western blots were performed as previously described (40). Protein was isolated using M-PER Mammalian Protein Extraction Reagent (Thermo Fisher Scientific), and Halt Protease and Phosphatase Inhibitor Cocktail (Thermo Fisher Scientific). Protein was quantified using the Pierce BCA Protein Assay Kit (Thermo Fisher Scientific), and 10 µg electrophoresed in 4–12% Bis-Tris denaturing gels (Thermo Fisher Scientific) using MOPS buffer chemistry (Thermo Fisher Scientific). Transfer was to 0.2 µm pore PVDF membranes (Bio-Rad Laboratories, CA, USA). Membranes were blocked in 5% skim milk for mouse anti-Actin-β (1:10,000, Sigma-Aldrich, #A1978), rabbit anti-ATG5 (1:2000, AbCam, Cambridge, UK, #ab108327), rabbit anti-Poly-(ADP-ribose) polymerase (**PARP**; 1:3,000, Cell Signaling Technology, Danvers, MS, USA, #9542), mouse anti-NRB1 (1:500, Thermo Fisher Scientific, # H00004077), and rabbit anti-Optineurin (**OPTN**; 1:2000, Cell Signaling Technology, #58981). Blocking with 5% bovine serum albumin (Merck, 126575) was used for rabbit anti-LC3B-I/II (1:3000, Cell Signaling Technology, #4108), rabbit anti-p62/Seqestosome-1 (**p62/SQSTM1**; 1:3000, Cell Signaling Technology, #5114), rabbit anti-TAX1BP1 (**TAX**; 1:2000, Cell Signaling Technology, #5105), rabbit anti-NDP52 (1:4000, Cell Signaling Technology, #60732), rabbit anti-pMTOR^{2448} (1:1000, Invitrogen, MA, USA, # 441125G), and rabbit anti-SIRT-1 (1:1000, AbCam, #ab7343). Membranes were subsequently probed overnight at 4°C with the same respective buffer/antibodies combinations. Secondary incubation was 1 h at ambient temperature in 5% skim milk with mouse or rabbit IgG horseradish peroxidase-conjugated antibodies (R&D Systems, MN, USA, #HAF007 and #HAF008, respectively). The suspension for blocking and antibody incubations was 1× Tris buffered saline (Thermo Fisher Scientific), with 0.1% Tween 20 (Merck). Where possible, outcomes were derived from a single transfer membrane for the respective replicate experiments to minimise inconsistencies produced by inter-blot variation. Chemiluminescent signal production was with Amersham ECL Advanced Western Blotting Detection reagents (GE Healthcare, IL, USA). Image acquisition was performed using the LAS-4000 Luminescent Image Analyzer (Fujifilm Life Sciences, Japan), with signal detection set to annotate blots beyond the linear range (depicted by pink-purple colour). Histogram densitometry was performed using Multi Gauge software (Fujifilm Life Sciences, V3.1, Japan).

Quantification of secreted IL-6

IL-6 secretion from THP-1-derived macrophages was quantified in the growth media using enzyme-linked immunosorbent assay (ELISA; Invitrogen, #BMS213INST) following the manufacturer's protocol.

Quantification of minimum inhibitory concentration (MIC)

Assessment of MIC was conducted as previously described (37), and in accordance with the Clinical and Laboratory Standards Institute guidelines (41). Briefly, log phase (OD 0.3-0.5, 600 nm) methicillin sensitive *S. aureus* (**MSSA**; ATCC 25923) was diluted in Mueller Hinton broth to a final inoculum of 5×10^5 CFU/well and added to 96-well plates containing a two-fold concentration gradient of antibiotics (0-128 µg/mL). Cultures were incubated for 16 h at 37°C and cell growth quantified (OD 630 nm; t_{16}-t_0 h background subtraction), in a 96-well plate reader (BioTek, Potton Bedfordshire, UK).

Statistical Methods

A Bayesian gamma (log link) generalised linear mixed model (**GLMM**) was applied (for the respective experiments/outcomes), to account for individual random effects for each sample, and target specific variances. For the transcript analysis, qRT-PCR data was incorporated into a single multi-gene model and multi-gene normalization was performed with the endogenous controls *18S rRNA*, hydroxymethylbilane synthase (*HMBS*) and TATA-box binding protein (*TBP*). Results were expressed as $\log_2$ (relative expression). For each protein, Western blot densitometry results were analysed with a random effect of test repetition and reported relative to the abundance of Actin-β. For the bacterial growth assay, effects of AZM and AZM-[O] on MIC, at each antibiotic concentration, were evaluated. To assess the anti-inflammatory potential of AZM-[O], the effect of treatment*exposure-time interaction on IL-6 secretion was assessed using GLMMs with measurement timepoint (hours) included as a repeated measure. Separate analyses were performed for the 1 and 10 ng/mL LPS-stimulated THP-1 macrophage models. Statistical analyses were performed using R (v 4.0.5) for the qPCR outcomes and IBM SPSS (v28.0.1.0) for the Western blot, MIC, and IL-6 secretion data.

Results

COPD exhibits a transcript profile indicative of autophagic insufficiency.

Clinically derived COPD and control bronchial biopsies (participant demographics shown in **Table 1**) were compared for the relative activity of autophagy regulatory and effector genes and transcript markers of airway inflammation. Of note, the variability (around the observed effect size) of the autophagy transcripts displayed remarkable stability across the study groups, particularly compared to the various inflammatory markers (**Fig. 1**). Delineating between the study groups, the abundance of autophagy-related transcripts showed a tendency for significant downregulation in the COPD group *vs* the outcomes for the controls. Most notably, the transcription factor *GATA1*, an influential driver of autophagy gene activity exhibited a 7.69-fold reduction for the COPD cohort ($P<0.001$, *vs* controls). With the notable exceptions of a reduction in *TSLP* (4.00-fold *vs* controls; $P=0.001$), and a trend for less *IL33* (1.75-fold *vs* controls; $P=0.067$), the outcomes for inflammation were consistent with a transcript profile for epithelial cells in the context of COPD. Further to this, the upregulation of *ICAM-1* expression was concordant with a chronic injury phenotype and heightened microbial surveillance that is observed in the COPD airway. Hence, these outcomes support a scenario of autophagic dysregulation at an airway epithelium managing exogenous COPD-related exposures (e.g., the factors in cigarette smoke) and chronic inflammation in the pulmonary tissues. It is noteworthy therefore that AZM, which is routinely prescribed to manage COPD, is a poorly recognised yet potent inhibitor of autophagy.

Table 1: Participant Demographics

Study Group	Gender	Age	FEV1/FVC (%)
Control	M	62	93
	M	38	104
	M	49	94
	M	42	93
	F	51	85
	F	58	88
COPD	M	71	46
	M	63	52
	M	59	71
	M	53	62
	M	62	63
	F	63	67
	F	60	58
	F	51	66
	F	65	64

The structural modifications required to synthesize azithromycin from erythromycin inhibit autophagy.

Initially, we tracked the structure-activity relationship of AZM *vs* autophagy in 16HBE14o- cells, in comparison to ERM and two intermediate macrolide derivatives, ERM-oxime and ERM-ether, that are commonly encountered along the synthetic pathway from ERM to AZM (refer to **Fig. 2A** for macrolide structures). Using the abundance of LC3B-II and p62/SQSTM1 as a readout of autophagic flux, we observed a concomitant and progressive increase in the LC3B-II/p62SQSTM1 signal for ERM and ERM-oxime, and a progressive and more significant increase for ERM-ether and

AZM. AZM demonstrated the largest effect size for autophagic blockade (i.e. accumulation of LC3B-II +30.7-fold, $P<0.001$ and p62/SQSTM1 +6.8-fold, $P<0.001$, *vs* control; **Fig. 2B-C**). In support of this outcome, our early observations show that chemical inhibitors of the mTORC1/2 complexes (Ku-00063796 and Torin-1) can counter the off-target block of autophagy caused by AZM (**Supp Fig. 1**). Further, tracking the fluorescently labelled AZM analogue (9a-NBD-azithromycin (31)) in 16HBE14o- cells treated with Ku-00063796, showed that this outcome is associated with a redistribution of lysosomes from the perinuclear region to the periphery of the cell (i.e. signals for lysosomes remain concentrated near the nucleus when autophagy is blocked (42); **Supp Fig. 2**). Subsequently, we expanded our library to include other clinically used semisynthetic macrolides produced from ERM, including CLM, ROX and TLM, all of which elicited a similar, albeit less pronounced accumulation of LC3B-II and p62/SQSTM1 (*vs* AZM). Observations during routine microscopy showed that each culture/exposure was morphologically comparable to the control, suggesting toxicity was not an obvious contributor to the outcomes for autophagy. For AZM, this was supported by non-significant outcomes for the abundance of cleaved PARP (i.e. caspase-3 activity), while the abundance of cleaved PARP due to the other (clinical) macrolides were marginally higher than the observed background level of programmed cell turnover. We also assessed the fourth-generation pre-clinical macrolide SLM, which displayed unique behaviour compared to the other macrolides, causing significant cell death and detachment (PARP +2.52-fold, $P=0.003$). The disproportionately high pro-apoptotic effect elicited by SLM is not fully comported here due to signal-loss of cleaved PARP as a result of cell detachment. This is evidenced by a large reduction in its corresponding Actin-β signal (3.23-fold lower than the average Actin-β signal of the other exposures; $P<0.001$). Only Rubicon and SIRT-1, which have roles in the positive regulation of programmed cell death, produced detectable/consistent signals for the SLM exposure. Notably, and excluding outcomes for SLM, while the expression of LC3B-II and p62/SQSTM1 (effectors of autophagy) demonstrated significant signal modulation (*vs* the control exposure), expression of the upstream pro-autophagy factors p-mTOR^{S2448}, Rubicon, SIRT1 and ATG5, were not significantly influenced by either macrolide in the context of this model. Also of note, probing p-mTOR^{S2448} in 16HBE14o- lysates provided two distinct signals of equivalent intensity, at 250 and 288 kDa. Hence, we designated both "p-mTOR^{S2448}" because, 1) both are confirmed by the manufacturer (albeit using different cell lysates), 2) related studies (to our knowledge) only report one or the other signal, 3) and, in any event, we did not observe signal modulation for p-mTOR^{S2448} using the exposures applied here. The significant effect on autophagic blockade observed with AZM, when compared to the other macrolides tested, was attributed to its unique physicochemical characteristics. Specifically, the dibasic nature and net charge of AZM at lysosomal pH values (**Supp. Table 2**) resulting in high lysosomal accumulation through ion trapping (30) is known to induce phospholipidosis (43), and is a likely contributor to autophagic inhibition.

Azithromycin causes the accumulation of autophagy receptors NBR1 and TAX to a greater degree than Optineurin and NDP52.

The various autophagy receptor proteins exhibit differential regulation and target specificity (e.g., depolarised mitochondria or intracellular microbes). Hence, we examined Neighbor of BRCA1 gene (NBR1), TAX1BP1 (TAX), Optineurin, and Nuclear dot protein 52 (NDP52), to identify any differential responses to the macrolides, and *vs* observations for p62/SQSTM1. For the treatments in the chemical synthetic pathway from ERM to AZM, the effect size for NRB1 and TAX abundance were strongly influenced by AZM (NBR1 +4.66-fold, $P<0.001$; TAX +8.68-fold, $P<0.001$; AZM *vs* control signal; **Fig. 3A-B**). Interestingly for NBR1 (and to a lesser extent TAX; but distinct to the

progressive elevation pattern seen in **Fig. 2B** for p62/SQSTM1), the elevation in this particular autophagy receptor was confined to the influences imparted by AZM and CLM, while neither of ERM, ERM-oxime, ERM-ether significantly modulated NRB1 (*vs* the control exposure). In comparison, the abundance of Optineurin and NDP52 remained relatively consistent across each condition, including for the other semisynthetic macrolides CLM, ROX and TLM. Indeed, the most significant influence imparted by CLM, ROX and TLM (when compared to all others) was the upregulation of NBR1. Of note however (and observed for the first time to our understanding), AZM was not the most influential exposure; CLM had a greater effect for NBR1, and each of CLM, ROX and TLM increased Optineurin beyond observations for AZM (albeit, neither were significantly larger). Given that the previous outcomes for SLM align with programmed cell death (**Fig. 2B-C**), its influence here for the autophagy receptors (i.e. depletion of a stable/detectable signal), suggests NBR1, TAX, Optineurin and NDP52 do not participate in the positive regulation of apoptosis in the context of this model (at least, as this relates to modulation of their protein abundance). Taken together, these outcomes support a salient effect of AZM to also prolong the duration (and thereby increase the abundance) of autophagy receptors other than p62/SQSTM1 within the cell (*vs* basal conditions in untreated cells). This effect was at least matched by other clinically relevant macrolides for particular autophagy receptors.

Modification of AZM's charged state significantly reduces its arrest of autophagy.

One mechanism for AZM inhibition of autophagy is entry into lysosomes where it becomes strongly protonated, depleting the local hydronium concentration, and leading to an increase in pH. Protonation of both the 9a-lactone and 3'-desosamine amine groups resulting in a double net positive charge effectively 'traps' AZM enabling this lysosomotropic effect. To confirm that the arrest of autophagy results from this mechanism we synthesised AZM-[O] by oxidising the desosamine group, thereby eliminating its ability to become protonated and therefore reducing the overall net charge of the molecule *vs* AZM (**Fig. 4A; Supp Table 2**). At the highest test concentration (50 µg/mL), oxidation of the desosaminyl amine appreciably lowered the accumulation of both LC3B-II and p62/SQSTM1 in 16HBE14o- cells (AZM-[O] *vs* AZM, -22.07-fold and -2.88-fold, respectively, both $P<0.001$; **Fig. 4B-C**). Examining the dose titration, both compounds elicited similar effects for the accumulation LC3B-II and p62/SQSTM1 for the 2.5 µg/mL intervention but became distinct at five times this amount (10 µg/mL, $P>0.05$). Of note, here the observations for cleaved PARP (apoptosis induction) grouped to produce an overall elevated outcome (*vs* outcomes in **Fig. 2**), for 10 and 50 µg/mL of AZM (2.31-fold, $P=0.004$ and 3.96-fold, $P<0.001$, respectively, *vs* control). While this agrees with inhibiting the pro-survival influences imparted by autophagy, routine microscopic observations showed the cells were not morphologically distinct from the control exposure.

Oxidation of the AZM desosamine group reduces its bacteriostatic activity.

We assessed the MIC for dose titrations of AZM and AZM-[O] to determine whether the oxidation of AZM desosaminyl amine modulates the bacteriostatic activity observed for AZM. Shown in **Fig. 5**, AZM exhibited exceptionally effective bacteriostatic activity, inhibiting the growth of the MSSA reference strain at an MIC within 1-4 µg/mL. In contrast the antimicrobial activity of AZM-[O] was significantly attenuated and was only able to affect a bacteriostatic outcome at the maximum exposure of 128 µg/mL. This outcome is consistent with the essential function of the tertiary amine of the AZM desosamine group as an important structural determinant that enables its inhibition of the bacterial 50S ribosomal subunit.

AZM-[O] exhibits attenuated anti-inflammatory properties *vs* AZM.

One beneficial off-target influence imparted by AZM is a moderate anti-inflammatory effect. To determine whether AZM-[O] retained this anti-inflammatory property, we quantified the magnitude of secreted IL-6 in an LPS-stimulated THP-1 macrophage model, co-exposed to either AZM or AZM-[O]. AZM significantly moderated the secretion of IL-6 when THP-1 macrophages were treated with 1 ng/mL LPS for the 6 and 24 h exposure intervals (-95.80 ng/mL, $P<0.001$ and -86.19 ng/mL, $P=0.002$, *vs* control, respectively; **Fig. 6A**), while AZM-[O] elicited a similar, albeit less influential effect (-22.55 ng/mL, $P<0.04$ and -55.37 ng/mL, $P=0.04$, *vs* control, respectively). In contrast, outcomes for AZM-[O] with 10 ng/mL LPS for either time interval were indiscernible from the control exposure (**Fig. 6B**). Interestingly, AZM was also less effective in the 10 ng/mL LPS model, with a significant outcome for the 6 h LPS exposure (-130.43 ng/mL, $P<0.001$, *vs* control), but a non-significant result for the 24 h model (-62.9 ng/mL, $P=0.161$, *vs* control). That AZM was also relatively less effective for the 24 h interval with 1 ng/mL LPS (*vs* the 6 h interval), hints to a washout mechanism possibly related to chemical stability within the cell, and/or the turnover of organelles and secretion of vesicles containing AZM.

Discussion

There is an emerging medical crisis due to bacteria becoming resilient to our frontline antibiotics. This problem is coupled with an apparent lack of urgency to develop new antibiotics to address this issue (35). AZM is exceptionally effective, but there are increasing calls to develop regulatory regimes to combat the emergence of AZM tolerant species (e.g., (44)). Given these issues, it is surprising that there is a paucity of information that describes AZM's potent off-target inhibition of autophagy – a fundamental survival process that also serves as the cells' bacterial clearance mechanism. COPD, bonchiectasis, CF and indeed most chronic respiratory diseases are driven by bacterial infections. Thus, supporting normal autophagy is crucial. Here we add to the body of understanding that supports a position that the factors regulating autophagy are suppressed in COPD, and demonstrate that AZM potently inhibits autophagy in human airway models. We also show that targeting its charged state (AZM-[O]) at the desosaminyl amine is one method to overcome this off-target effect.

Ostensibly, the consequences of arrested autophagy map to the features of COPD, such as nutrient deprivation, mitochondrial dysfunction (mitophagy), accelerated senescence and recalcitrant bacterial infection (xenophagy) (4, 22). Nevertheless, we are yet to realise a consensus (or convincing/prevailing argument) that can assert whether autophagy is increased as a maladaptive response in COPD, or inhibited, and thereby causing the aforementioned deficits (e.g., (23, 45)). The challenge is identifying a causal relationship between two nebulous phenomena; autophagy, a multifunctional biochemical process governed by numerous regulatory factors, and COPD, a complex condition combining autoimmune-like hyperreactions and gene-environment interactions (to name two). Further, quantifying autophagic function in the laboratory is uniquely challenging (and near impossible in humans), and COPD is difficult to diagnose in the clinic (e.g., (46, 47)). Hence, there is reason to be guarded when ascribing biological significance to discrete autophagy-related pathways/factors identified using bottom-up *in vitro* and animal models which, for reasons that are beyond this discussion, are far removed from COPD in humans. Recently, we have favoured top-down approaches to assess perturbations in autophagy using COPD/control studies. Our most recent investigation employed

a new organotypic method of assessing autophagy in human samples (48), and showed that autophagic flux is decreased in peripheral blood mononuclear cells from COPD (49). While there is no reason to doubt these findings, the major challenge for these inquiries (particularly over the past four years), is assembling large numbers of well-defined COPD/control participants, so the outcomes for autophagy are predictive of COPD (and its many endotypes). Compounding this, and as evidenced in **Fig 1**, measuring autophagy (and/or factors that govern autophagy) in a disease/control study design offers relatively modest the effect sizes (vs inflammatory factors, for example). This is in part because autophagy is strictly regulated and has a central role in cell viability and homeostasis. What's more, and specific to this study, our pool of COPD participants did not include an AZM sub-group due to ethical considerations related to sampling inpatients with current bacterial infection. Consequently, we opted for a widely recognised airway epithelial cell model for our assessments of AZM.

The comparative effects of different clinical and intermediate macrolides on autophagic flux provided some useful insights into SARs, particularly with respect to AZM, and possibly point towards novel modes of action for other macrolides. While the accumulation of AZM in the lysosome resulting from ion trapping of its doubly charged (2+) state correlates with autophagic inhibition, other macrolides also display upregulated levels of markers of autophagic arrest despite very different protonation states. Excluding SLM for obvious toxicological reasons, ERM-ether and TLM are the only other macrolides tested that have ionisable basic groups other than the desosamine group, which is common to all of the macrolides. Thus, the decrease in lysosomal pH relative to the cytosol could lead to an increase in the net charge (> 1+) of ERM-ether and TLM resulting in their retention (**Supp Table 2**), which may contribute to an increase in lysosomal pH and autophagic arrest, as observed for AZM. This is somewhat supported by the similarly high accumulation of TLM and AZM previously reported in polymorphonuclear neutrophils (50-52). In comparison, the accumulation of CLM and ROX in polymorphonuclear neutrophils is significantly lower, which is consistent with their lower net charge (≤ 1+). Nevertheless, CLM and ROX displayed upregulation of LC3B-II and p62/SQSTM1 similarly to TLM, suggesting an alternative (and/or an additional) mechanism of autophagic arrest for these macrolides. Unfortunately, calculation and comparison of the physiochemical properties of the macrolides did not provide any further insights that would explain these trends (**Supp Table 2**).

Related to this, we noted that the autophagy receptors exhibited differential abundance profiles, depending on which macrolide was applied to the model. This outcome, coupled with the duration (days) that macrolides can remain within the cellular environment, means they have an extended opportunity to perturb further and distinct autophagy-related factors beyond the arrest of autophagosome-lysosome fusion (51, 52). One possibility is that the macrolide-dependent differences arise due to distinct influences on the factors that govern the unique post-translational modifications observed for the various autophagy receptors (53). More generally, they may modulate the numerous up-stream regulators of the autophagy pathway (e.g. 51), and/or the overlapping cellular processes that influence autophagy during (for example) innate immunity and cells survival (noted here with our observations for PARP/apoptosis). To address these complexities for AZM, we have developed an AZM photoaffinity probe to track signals emitted from a photoreactive group that occur when the probe covalently crosslinks with proteins within the cell. The outcomes will be used to, 1) map the AZM-protein interactome (with a focus on autophagy) in models of the human airway, 2) inform the development of further AZM-derivatives, and 3) functionally validate derivatives that mitigate the arrest of autophagy and that retain the immunomodulatory effects observed for the parent molecule.

One such AZM derivative we assessed here was AZM-[O]. We predicted AZM-[O]'s altered charge state (vs AZM) would mitigate the off-target inhibition of autophagy observed for the parent molecule. While this outcome was realised, this particular modification (oxidation of the desosaminyl amine) also significantly diminished the antibacterial and anti-inflammatory activities observed with AZM. An ideal outcome would have been a derivative that corrected the off-target block of autophagy, was nonantibiotic, but that retained its immunomodulatory activity. Such a derivative would provide an invaluable non-steroidal anti-inflammatory that concentrates at the airways, without contributing to the selection of AZM-resistance bacteria (54). The challenge here is that AZM's unique anti-inflammatory effect(s) await a clear description (55), and we suspect these properties are mediated (and hidden amongst) intricate cell-cell interactions at the organ level e.g. during the type of inflammation synonymous with COPD. For autophagy, AZM has been noted to indirectly influence the mTOR pathway (via inhibition of S6RP phosphorylation) in the context of idiopathic bronchiolitis, albeit with a high concentration of AZM (300 µg/mL) (56). However, no studies have attempted to identify specific lysosomal ion channel or transporter binding domains that could inform SAR studies to address AZM-mediated suppression of autophagosome-lysosome fusion. The most promising nonantibiotic AZM derivative reported thus far (to our knowledge) was by Kragol et al. (2022), who synthesized a stereoisomer of AZM that retained significant immunomodulatory activity, albeit the suppressive effects on autophagy were not examined (57). Nevertheless, the combination this outcome with ours for AZM-[O] provide promising evidence that the structural determinants of AZM's antibacterial activity, and the off-target effects for autophagy and innate immunity, may be mutually exclusive.

In this study, we demonstrate that the potent inhibition of autophagy by AZM is not unique to this macrolide antibiotic. This finding raises critical questions about other antibiotics that may have deleterious effects on mammalian cells, potentially limiting their long-term utility. Uncovering the full spectrum of off-target effects is not only essential to safeguard the efficacy of critically important antibiotics for future generations, but also serve as a discover pathway for urgently needed alternative compounds with enhanced therapeutic potential.

Acknowledgements

We are grateful for the expertise and support of the clinical staff of the Royal Adelaide Hospital Thoracic Department, The Queen Elizabeth Hospital Respiratory Unit and the participants enrolled into this study who generously provided their valuable time and tissue samples. We are also thankful for the pharmacological insight provided by Prof Benedetta Sallustio (University of Adelaide) and assistance in chemical synthesis by Christian Danker (University of South Australia). This study was funded by the Royal Adelaide Research Committee, Royal Adelaide Hospital Research Fund, The Health Services Charitable Gifts Board, and the Rebecca L Cooper Medical Research Foundation.

Disclosure statement.

The authors have no COI to disclose.

Figure legends.

Figure 1: Autophagy gene activity is reduced in COPD.

Transcript abundance of key positive regulators of autophagy are downregulated in COPD (n=9, age 60.8 ± SD 6.06, FEV1/FVC 64.5 ± SD 4.51) *vs* control (n=6, age 50.0 ± 9.14 SD, FEV1/FVC 92.83 ± 6.49 SD) bronchial brushing biopsies. With some exceptions (notably *TSLP* and *IL-33*), these changes are associated with an upregulation of inflammatory and cell adhesion transcripts. Magnitudes are expressed as COPD *vs* control (i.e., less/more transcript abundance in COPD-derived samples to the left/right of zero, respectively), and ordered to highlight transcript groups related to gene-dependent variation. Dashed vertical lines for $\log_2$ (relative expression) at – 2.0 correspond to a fold-change of 0.25, and +2.0 correspond to a fold-change of 4.0. Results are normalized to three reference genes and are significant to at least $P<0.05$ when 95% confidence interval (CI) do not cross zero.

Figure 2: Azithromycin causes a heightened autophagic arrest response in human airway epithelial cells compared to its precursor compounds and related macrolide antibiotics.

A. Chemical structures of the macrolides. Chemical structures of erythromycin A (**ERM**), erythromycin-9-oxime (**ERM-oxime**), erythromycin-9,11-imino ether (**ERM-ether)**, azithromycin (**AZM**), clarithromycin (**CLM**), roxithromycin (**ROX**), telithromycin (**TEL**) and solithromycin (**SLM)** with systematic numbering of the aglycone lactone, desosamine and cladinose rings provided in red, green and blue, respectively. The lactone macrocyclic ring (numbering system indicates carbon/nitrogen bonds) is bonded with a desosamine sugar group (upper five carbon ring moiety bound through AZM C5) for each antibiotic and the cladinose sugar (lower five carbon ring moiety bound through AZM C3) for each except TEL and SOL. **B.** 16HBE14o- cell responses to the macrolide exposures (16 h, 50 µg/mL). Outcomes represent n=3 independent cultures/Western blots. Outcomes for the target proteins that demonstrated significant response/modulation to the exposure(s) are shown. Outcomes for each of the respective n=3 repeated measures of the targets were derived from a single transfer membrane to minimise inconsistencies produced by inter-blot variation. Expressions was normalized to Actin-β. Effect sizes represented fold-change relative to the control treatment and uncertainty intervals are ± 95% CI. Results are significant to at least $P<0.05$ when 95% CI do not cross the dashed line (1-fold). Vehicle (VEH) is ≤ 0.1% DMSO *vs* culture volume. **C.** Western blot showing protein signals derived from the 16HBE14o- model exposed to the various macrolides (16 h, 50 µg/mL). Large and concomitant

increase in LC3B-II and p62/SQSTM1 abundance for the AZM exposure (*vs* control), indicates a heightened arrest of autophagic flux (i.e. reduced autolysosomal turnover). This effect appears to be independent of alteration in protein abundance of influential up-stream pro-autophagy factors such as p-mTOR^{S2448} and SIRT1.

Figure 3: The autophagy receptors NBR1 and TAX are elevated by Azithromycin.

A. Quantification of the protein abundance measures for the autophagy receptors NBR1, TAX, Optineurin and NDP52 in 16HBE14o- cell exposed to the macrolides (16 h, 50 µg/mL). Effect sizes represent n=3 independent cultures/Western blots. Outcomes for each of the respective repeated measures of the targets were derived from a single transfer membrane to minimise inconsistencies produced by inter-blot variation. Expressions was normalised to Actin-β. Effect sizes represented fold-change relative to the control treatment and uncertainty intervals are ±95% CI. Results are significant to at least $P<0.05$ when 95% CI do not cross the dashed line (1-fold). **B.** Western blot shows autophagy receptor protein signals from 16HBE14o- cultures exposed to the various macrolides (16 h, 50 µg/mL). Responses for NBR1 and TAX show significant signal modulation when the 16HBE14o- cells were exposed to AZM, but relatively less Optineurin (OPTN) and NDP52 was observed to accumulate as a result of this macrolide (*vs* the control exposure). Interestingly, CLM elicited a stronger (but not statistically distinct) effect for the elevation of NBR1 *vs* AZM, and each of CLM, ROX and TLM produced a similar outcome (*vs* AZM) for the autophagy receptor Optineurin.

Figure 4: Structure-activity relationship of AZM vs autophagy shows oxidation of the desosaminyl amine diminishes its off-target block of autophagy.

A. Scheme showing oxidation of AZM desosaminyl amine. Oxidation of the desosaminyl amine (blue circles) produces a zwitterionic *N*-oxide group (no net charge), blocking the potential protonation of the amine group. **B.** Quantification of the outcomes of Western blot analyses shows the concomitant increase in the abundance of LC3B-II and p62/SQSTM1 for AZM is significantly reduced for the AZM-[O] derivative. The outcomes for AZM and LC3B-II / p62/SQSTM1 follow a dose relationship (2.5, 10, and 50 µg/mL; 16 h). Here, this outcome is matched by a progressive increase in apoptosis with AZM (as assess via the abundance of cleaved PARP), which is not observed after exposure with the oxidised form. Expressions was normalized to Actin-β. Effect sizes represented fold-change relative to the control treatment and uncertainty intervals are ±95% CI. Results are significant to at least $P<0.05$ when 95% CI do not cross the dashed line (1-fold). **C.** Representative Western blot shows the processing of PARP to produce cleaved PARP, and the concomitant progressive elevation of LC3B-II and p62/SQSTM1 in 16HBE14o- cells after stimulation with increasing concentrations of AZM, but which is not observed for AZM-[O]. Actin-β served as the loading control.

Figure 5: AZM-[O] exhibits low bacteriostatic efficacy vs the AZM parent molecule.

MSSA was used to model the comparative bacteriostatic potential of AZM *vs* the AZM-[O] derivative. AZM was extremely effective in preventing the growth of MSSA (MIC of approximately 2 µg/mL over a 16 hour assay period), whereas AZM-[O] approached MIC at the maximum dose of 128 µg/mL (over 64-fold reduction in bacteriostatic activity *vs* AZM). The bacteriostatic effect of AZM-[O] was approximately 105% lower than AZM at every exposure dose ($P<0.001$). Outcomes represent n=7 replicate experiments; shaded area represents ±SD.

Figure 6: Oxidation of AZM desosaminyl amine attenuates its anti-inflammatory activity.

The secretion of IL-6 was used to assess the anti-inflammatory effect imparted by AZM *vs*. AZM-[O]. THP-1 macrophages stimulated with LPS respond by secreting IL-6 into the media, particularly for the 6 and 24 hour time period. AZM's reduction of IL-6 was most evident after co-exposure with 1 ng/mL LPS for the 6 and 24 hour treatment intervals, and to a similar extend for 10 ng/mL LPS after 6 hours. In contrast, AZM-[O] exhibited a significantly attenuated effect for the reduction of secreted IL-6 (*vs* the parent molecule) with 1 ng/mL LPS, and outcomes using 10 ng/mL LPS were comparable to the control exposure. Outcomes represent n=3 separate experiments; confidence intervals are ±SD.

Supp Fig 1: Chemical inhibitors of mTORC1/2 can counter AZM's block of autophagy.

16HBE14o- cells were exposed to 10 or 50 µg/mL AZM and increasing concentrations of the chemical blockers of mTOCR1/2, Ku-0063794 ("KU") and Torin-1 (both 16 hour co-treatment). Western blot outcomes show a reduction in LC3B-II and p62/SQSTM1 abundance that follows a dose relationship for increasing concentrations of the mTORC1/2 inhibitors, which is particularly evident for the 50 µg/mL AZM co-exposure model. This outcome was also noted for the autophagy receptor TAX1BP1. These outcomes suggest a partial restoration of autophagic flux by overcoming the potent block imposed by AZM. Outcomes for each respective target (representative of n=2 blots) were derived from a single transfer membrane to minimise inconsistencies produced by inter-blot variation. Actin-β served as a loading control.

Supp Fig 2: Ku-0063794 promotes redistribution of lysosomes from the perinuclear region by 9a-NBD-azithromycin to the cell periphery.

Lysosomes were loaded with 10 µg/mL the fluorescent AZM analogue 9a-NBD-AZM for 2 h in the 16HBE14o- cell model and then treated with the chemical inhibitor of mTORC1/2, Ku-0063794 (10 µM, 16 h after exposure to 9a-NBD-AZM). Confocal immunofluorescence microscopy shows the cells treated with 9a-NBD-AZM have lysosomes localised around the nucleus. Ku-0063794 promoted the redistribution of lysosomes loaded with the fluorescent AZM analogue to the periphery of the cells. This redistribution pattern from the centre (autophagic block via 9a-NBD-AZM) to the periphery (active autophagy) is indicative of the restoration of autophagic activity. Outcomes represent n=3 independent experiments.

Reference list.

1. Syamlal G, Kurth LM, Dodd KE, Blackley DJ, Hall NB, Mazurek JM. Chronic Obstructive Pulmonary Disease Mortality by Industry and Occupation - United States, 2020. MMWR Morb Mortal Wkly Rep. 2022;71(49):1550-4.
2. Viegi G, Maio S, Fasola S, Baldacci S. Global Burden of Chronic Respiratory Diseases. J Aerosol Med Pulm Drug Deliv. 2020;33(4):171-7.
3. Ramsheh MY, Haldar K, Bafadhel M, George L, Free RC, John C, et al. Resistome analyses of sputum from COPD and healthy subjects reveals bacterial load-related prevalence of target genes. Thorax. 2020;75(1):8-16.
4. Poh WP, Kicic A, Lester SE, Nguyen PT, Bakaletz LO, Reynolds PN, et al. COPD-Related Modification to the Airway Epithelium Permits Intracellular Residence of Nontypeable Haemophilus influenzae and May Be Potentiated by Macrolide Arrest of Autophagy. Int J Chron Obstruct Pulmon Dis. 2020;15:1253-60.
5. Liu X, Liu F, Ding S, Shen J, Zhu K. Sublethal Levels of Antibiotics Promote Bacterial Persistence in Epithelial Cells. Adv Sci (Weinh). 2020;7(18):1900840.
6. Rawlins EL, Hogan BL. Ciliated epithelial cell lifespan in the mouse trachea and lung. Am J Physiol Lung Cell Mol Physiol. 2008;295(1):L231-4.
7. Sethi S, Maloney J, Grove L, Wrona C, Berenson CS. Airway inflammation and bronchial bacterial colonization in chronic obstructive pulmonary disease. Am J Respir Crit Care Med. 2006;173(9):991-8.
8. Patel IS, Seemungal TA, Wilks M, Lloyd-Owen SJ, Donaldson GC, Wedzicha JA. Relationship between bacterial colonisation and the frequency, character, and severity of COPD exacerbations. Thorax. 2002;57(9):759-64.
9. Mao K, Klionsky DJ. Xenophagy: A battlefield between host and microbe, and a possible avenue for cancer treatment. Autophagy. 2017;13(2):223-4.
10. Tan WSD, Shen HM, Wong WSF. Dysregulated autophagy in COPD: A pathogenic process to be deciphered. Pharmacol Res. 2019;144:1-7.
11. Racanelli AC, Kikkers SA, Choi AMK, Cloonan SM. Autophagy and inflammation in chronic respiratory disease. Autophagy. 2018;14(2):221-32.
12. Mina MJ, Klugman KP. The role of influenza in the severity and transmission of respiratory bacterial disease. Lancet Respir Med. 2014;2(9):750-63.
13. Gordon RJ, Gordon RJ, De G, Gordon RJ, Gordon RJ. The Rise and Fall of American Growth : The U.S. Standard of Living since the Civil War. Princeton, NJ: Princeton University Press; 2017.
14. Stein SW, Thiel CG. The History of Therapeutic Aerosols: A Chronological Review. J Aerosol Med Pulm Drug Deliv. 2017;30(1):20-41.
15. Mukai S, Moriya S, Hiramoto M, Kazama H, Kokuba H, Che XF, et al. Macrolides sensitize EGFR-TKI-induced non-apoptotic cell death via blocking autophagy flux in pancreatic cancer cell lines. Int J Oncol. 2016;48(1):45-54.
16. Renna M, Schaffner C, Brown K, Shang S, Tamayo MH, Hegyi K, et al. Azithromycin blocks autophagy and may predispose cystic fibrosis patients to mycobacterial infection. J Clin Invest. 2011;121(9):3554-63.
17. Barnes PJ, Baker J, Donnelly LE. Cellular Senescence as a Mechanism and Target in Chronic Lung Diseases. Am J Respir Crit Care Med. 2019;200(5):556-64.
18. Roscioli E, Tran HB, Jersmann H, Nguyen PT, Hopkins E, Lester S, et al. The uncoupling of autophagy and zinc homeostasis in airway epithelial cells as a fundamental contributor to COPD. Am J Physiol Lung Cell Mol Physiol. 2017;313(3):L453-L65.
19. Dong LL, Liu ZY, Chen KJ, Li ZY, Zhou JS, Shen HH, Chen ZH. The persistent inflammation in COPD: is autoimmunity the core mechanism? Eur Respir Rev. 2024;33(171).
20. Cloonan SM, Lam HC, Ryter SW, Choi AM. "Ciliophagy": The consumption of cilia components by autophagy. Autophagy. 2014;10(3):532-4.
21. Ng Kee Kwong F, Nicholson AG, Harrison CL, Hansbro PM, Adcock IM, Chung KF. Is mitochondrial dysfunction a driving mechanism linking COPD to nonsmall cell lung carcinoma? Eur Respir Rev. 2017;26(146).
22. Barnes PJ, Burney PG, Silverman EK, Celli BR, Vestbo J, Wedzicha JA, Wouters EF. Chronic obstructive pulmonary disease. Nat Rev Dis Primers. 2015;1:15076.
23. Li ZY, Wu YF, Xu XC, Zhou JS, Wang Y, Shen HH, Chen ZH. Autophagy as a double-edged sword in pulmonary epithelial injury: a review and perspective. Am J Physiol Lung Cell Mol Physiol. 2017;313(2):L207-L17.
24. Liao SX, Sun PP, Gu YH, Rao XM, Zhang LY, Ou-Yang Y. Autophagy and pulmonary disease. Ther Adv Respir Dis. 2019;13:1753466619890538.
25. Heidary M, Ebrahimi Samangani A, Kargari A, Kiani Nejad A, Yashmi I, Motahar M, et al. Mechanism of action, resistance, synergism, and clinical implications of azithromycin. J Clin Lab Anal. 2022;36(6):e24427.

26. Labi AK, Obeng-Nkrumah N, Dayie N, Egyir B, Sampane-Donkor E, Newman MJ, Opintan JA. Antimicrobial use in hospitalized patients: a multicentre point prevalence survey across seven hospitals in Ghana. JAC Antimicrob Resist. 2021;3(3):dlab087.
27. McMullan BJ, Mostaghim M. Prescribing azithromycin. Aust Prescr. 2015;38(3):87-9.
28. Laux J, Martorelli M, Strass S, Schollmeyer D, Maier F, Burnet M, Laufer SA. Inherent Fluorescence Demonstrates Immunotropic Properties for Novel Janus Kinase 3 Inhibitors. ACS Pharmacol Transl Sci. 2023;6(10):1433-52.
29. Aubert JD, Juillerat-Jeanneret L, Fioroni P, Dayer P, Plan PA, Leuenberger P. Function of human alveolar macrophages after a 3-day course of azithromycin in healthy volunteers. Pulm Pharmacol Ther. 1998;11(4):263-9.
30. Derendorf H. Excessive lysosomal ion-trapping of hydroxychloroquine and azithromycin. Int J Antimicrob Agents. 2020;55(6):106007.
31. Matijasic M, Munic Kos V, Nujic K, Cuzic S, Padovan J, Kragol G, et al. Fluorescently labeled macrolides as a tool for monitoring cellular and tissue distribution of azithromycin. Pharmacol Res. 2012;66(4):332-42.
32. Nujic K, Banjanac M, Munic V, Polancec D, Erakovic Haber V. Impairment of lysosomal functions by azithromycin and chloroquine contributes to anti-inflammatory phenotype. Cell Immunol. 2012;279(1):78-86.
33. Zelmer AR, Nelson R, Richter K, Atkins GJ. Can intracellular Staphylococcus aureus in osteomyelitis be treated using current antibiotics? A systematic review and narrative synthesis. Bone Res. 2022;10(1):53.
34. Klug DM, Idiris FIM, Blaskovich MAT, von Delft F, Dowson CG, Kirchhelle C, et al. There is no market for new antibiotics: this allows an open approach to research and development. Wellcome Open Res. 2021;6:146.
35. Piddock LJ. The crisis of no new antibiotics--what is the way forward? Lancet Infect Dis. 2012;12(3):249-53.
36. Gene M. Bright G, Conn. , inventor; Sandoz AG, Basel (CH), assignee. Derivatives of azithromycin. United States1984.
37. Guo T, Chen Y, Chen W, Semple SJ, Gu X, Polyak SW, et al. Design and synthesis of benzochromene derivatives as AcrB inhibitors for the reversal of bacterial multidrug resistance. Eur J Med Chem. 2023;249:115148.
38. Hamon R, Tran HB, Roscioli E, Ween M, Jersmann H, Hodge S. Bushfire smoke is pro-inflammatory and suppresses macrophage phagocytic function. Sci Rep. 2018;8(1):13424.
39. Pinto SM, Kim H, Subbannayya Y, Giambelluca MS, Bosl K, Ryan L, et al. Comparative Proteomic Analysis Reveals Varying Impact on Immune Responses in Phorbol 12-Myristate-13-Acetate-Mediated THP-1 Monocyte-to-Macrophage Differentiation. Front Immunol. 2021;12:679458.
40. Delhove J, Alawami M, Macowan M, Lester SE, Nguyen PT, Jersmann HPA, et al. Organotypic sinonasal airway culture systems are predictive of the mucociliary phenotype produced by bronchial airway epithelial cells. Sci Rep. 2022;12(1):19225.
41. Humphries RM, Miller L, Zimmer B, Matuschek E, Hindler JA. Contemporary Considerations for Establishing Reference Methods for Antibacterial Susceptibility Testing. J Clin Microbiol. 2023;61(6).
42. Jahreiss L, Menzies FM, Rubinsztein DC. The itinerary of autophagosomes: from peripheral formation to kiss-and-run fusion with lysosomes. Traffic. 2008;9(4):574-87.
43. Van Bambeke F, Montenez JP, Piret J, Tulkens PM, Courtoy PJ, Mingeot-Leclercq MP. Interaction of the macrolide azithromycin with phospholipids. I. Inhibition of lysosomal phospholipase A1 activity. Eur J Pharmacol. 1996;314(1-2):203-14.
44. Mack I, Sharland M, Berkley JA, Klein N, Malhotra-Kumar S, Bielicki J. Antimicrobial Resistance Following Azithromycin Mass Drug Administration: Potential Surveillance Strategies to Assess Public Health Impact. Clin Infect Dis. 2020;70(7):1501-8.
45. Mizumura K, Cloonan S, Choi ME, Hashimoto S, Nakahira K, Ryter SW, Choi AM. Autophagy: Friend or Foe in Lung Disease? Ann Am Thorac Soc. 2016;13 Suppl 1(Suppl 1):S40-7.
46. Klionsky DJ, Abdel-Aziz AK, Abdelfatah S, Abdellatif M, Abdoli A, Abel S, et al. Guidelines for the use and interpretation of assays for monitoring autophagy (4th edition)(1). Autophagy. 2021;17(1):1-382.
47. Weiss ST, DeMeo DL, Postma DS. COPD: problems in diagnosis and measurement. Eur Respir J Suppl. 2003;41:4s-12s.
48. Bensalem J, Hattersley KJ, Hein LK, Teong XT, Carosi JM, Hassiotis S, et al. Measurement of autophagic flux in humans: an optimized method for blood samples. Autophagy. 2021;17(10):3238-55.
49. Cooper JM, Chen S, Lester SE, Kim J, Gummow J, Crowhurst T, et al. Autophagy is suppressed in peripheral blood mononuclear cells during chronic obstructive pulmonary disease. bioRxiv. 2024:2024.04.27.591479.
50. Blandizzi C, Malizia T, Batoni G, Ghelardi E, Baschiera F, Bruschini P, et al. Distribution of azithromycin in plasma and tonsil tissue after repeated oral administration of 10 or 20 milligrams per kilogram in pediatric patients. Antimicrob Agents Chemother. 2002;46(5):1594-6.

51. Labro MT. Intracellular bioactivity of macrolides. Clin Microbiol Infect. 1996;1 Suppl 1:S24-S30.
52. Vazifeh D, Preira A, Bryskier A, Labro MT. Interactions between HMR 3647, a new ketolide, and human polymorphonuclear neutrophils. Antimicrob Agents Chemother. 1998;42(8):1944-51.
53. Gubas A, Dikic I. A guide to the regulation of selective autophagy receptors. FEBS J. 2022;289(1):75-89.
54. Mencarelli A, Distrutti E, Renga B, Cipriani S, Palladino G, Booth C, et al. Development of non-antibiotic macrolide that corrects inflammation-driven immune dysfunction in models of inflammatory bowel diseases and arthritis. Eur J Pharmacol. 2011;665(1-3):29-39.
55. Slater M, Torr E, Harrison T, Forrester D, Knox A, Shaw D, Sayers I. The differential effects of azithromycin on the airway epithelium in vitro and in vivo. Physiol Rep. 2016;4(18).
56. Weng D, Wu Q, Chen XQ, Du YK, Chen T, Li H, et al. Azithromycin treats diffuse panbronchiolitis by targeting T cells via inhibition of mTOR pathway. Biomed Pharmacother. 2019;110:440-8.
57. Kragol G, Steadman VA, Marusic Istuk Z, Cikos A, Bosnar M, Jelic D, et al. Unprecedented Epimerization of an Azithromycin Analogue: Synthesis, Structure and Biological Activity of 2'-Dehydroxy-5''-Epi-Azithromycin. Molecules. 2022;27(3).

Fig. 1

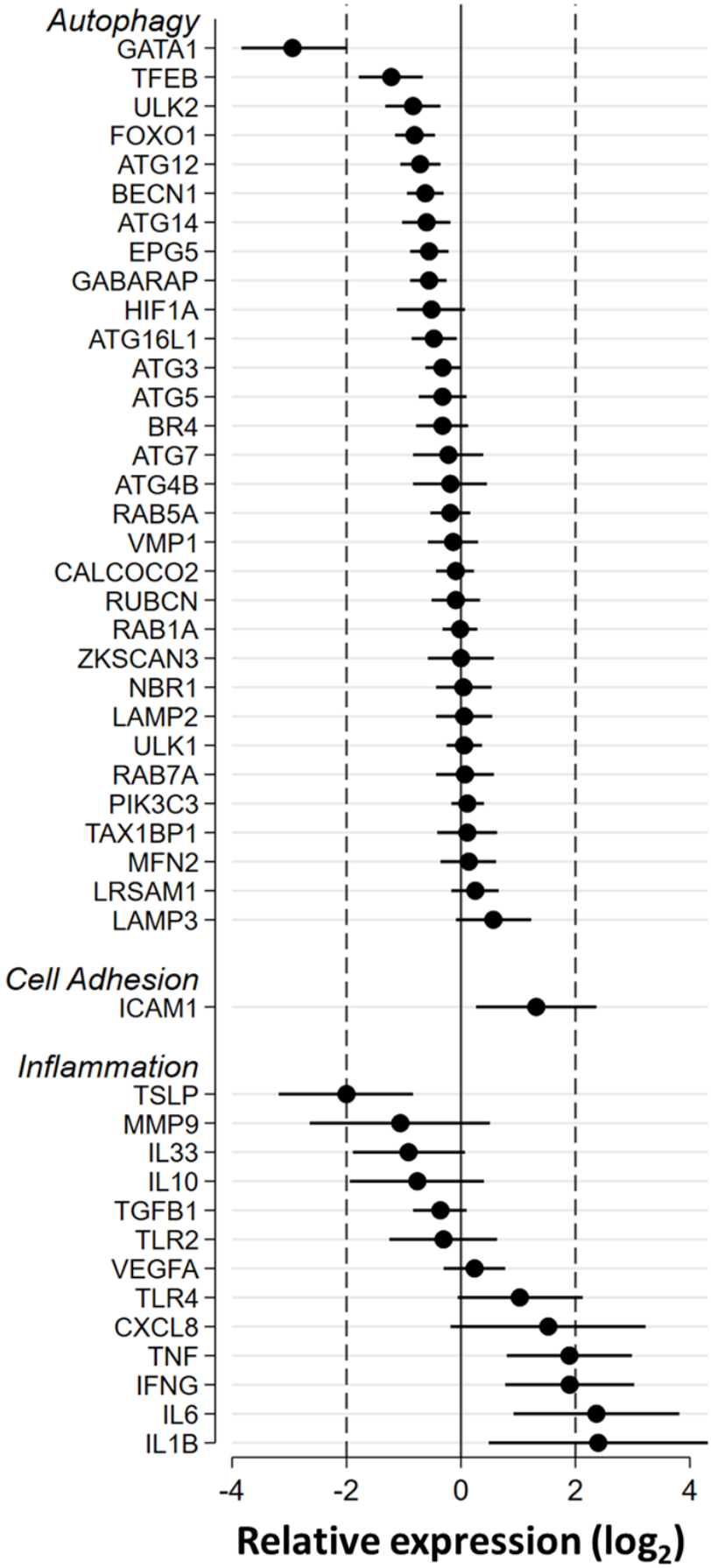
Autophagy
GATA1
TFEB
ULK2
FOXO1
ATG12
BECN1
ATG14
EPG5
GABARAP
HIF1A
ATG16L1
ATG3
ATG5
BR4
ATG7
ATG4B
RAB5A
VMP1
CALCOCO2
RUBCN
RAB1A
ZKSCAN3
NBR1
LAMP2
ULK1
RAB7A
PIK3C3
TAX1BP1
MFN2
LRSAM1
LAMP3
Cell Adhesion
ICAM1
Inflammation
TSLP
MMP9
IL33
IL10
TGFB1
TLR2
VEGFA
TLR4
CXCL8
TNF
IFNG
IL6
IL1B
-4
-2
0
2
4
Relative expression (log2)

Fig. 2

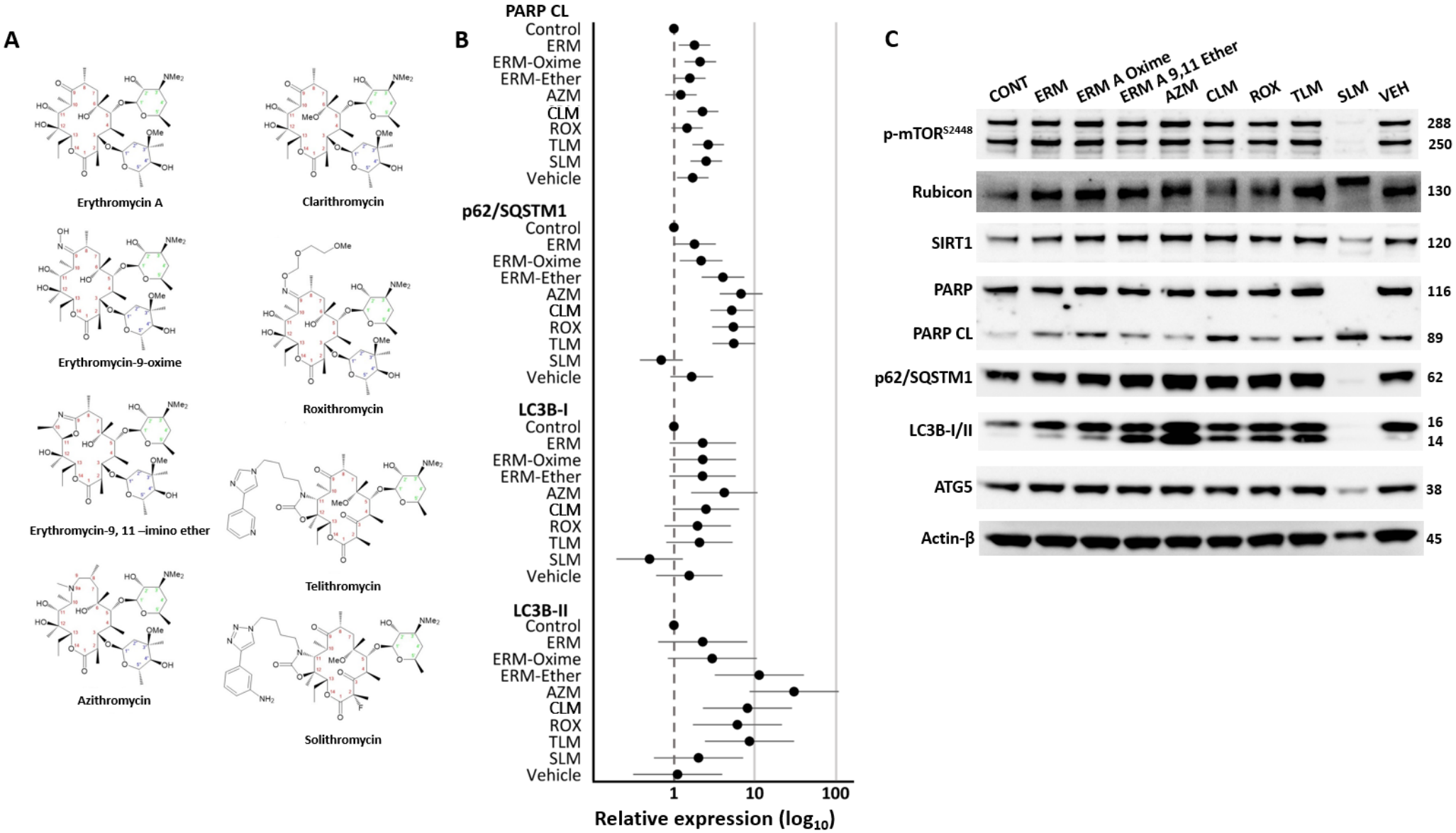
A
Erythromycin A
Clarithromycin
Erythromycin-9-oxime
Roxithromycin
Erythromycin-9, 11 –imino ether
Telithromycin
Azithromycin
Solithromycin
B
PARP CL
p62/SQSTM1
LC3B-I
LC3B-II
Control
ERM
ERM-Oxime
ERM-Ether
AZM
CLM
ROX
TLM
SLM
Vehicle
1
10
100
Relative expression (log10)
C
CONT
ERM
ERM A Oxime
ERM A 9,11 Ether
AZM
CLM
ROX
TLM
SLM
VEH
p-mTOR S2448
288
250
Rubicon
130
SIRT1
120
PARP
116
PARP CL
89
p62/SQSTM1
62
LC3B-I/II
16
14
ATG5
38
Actin-β
45

Fig. 3

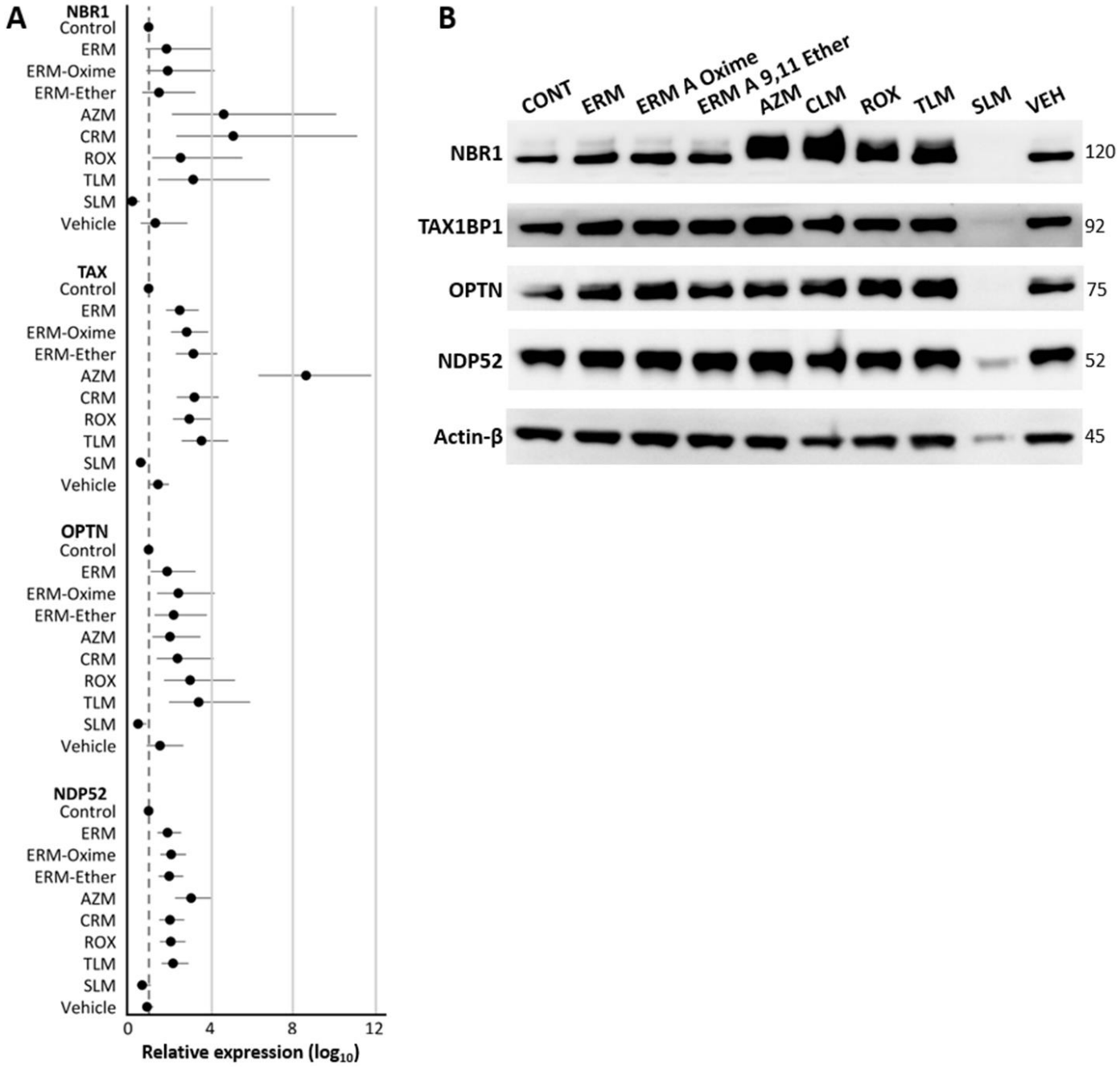
A
NBR1
Control
ERM
ERM-Oxime
ERM-Ether
AZM
CRM
ROX
TLM
SLM
Vehicle
TAX
Control
ERM
ERM-Oxime
ERM-Ether
AZM
CRM
ROX
TLM
SLM
Vehicle
OPTN
Control
ERM
ERM-Oxime
ERM-Ether
AZM
CRM
ROX
TLM
SLM
Vehicle
NDP52
Control
ERM
ERM-Oxime
ERM-Ether
AZM
CRM
ROX
TLM
SLM
Vehicle
0
4
8
12
Relative expression (log10)
B
CONT
ERM
ERM A Oxime
ERM A 9,11 Ether
AZM
CLM
ROX
TLM
SLM
VEH
NBR1
120
TAX1BP1
92
OPTN
75
NDP52
52
Actin-β
45

Fig. 4

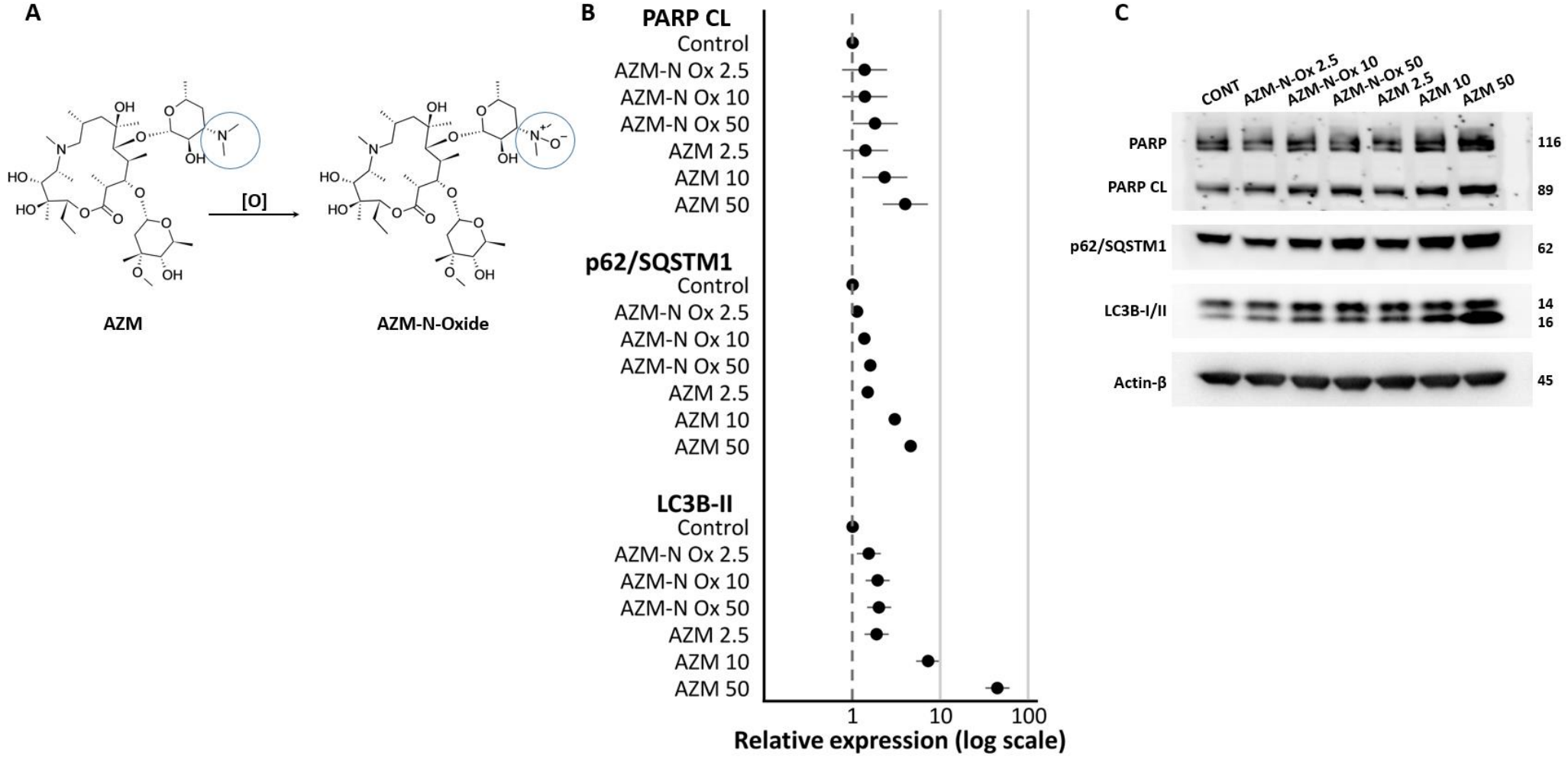
A
[O]
AZM
AZM-N-Oxide
B
PARP CL
Control
AZM-N Ox 2.5
AZM-N Ox 10
AZM-N Ox 50
AZM 2.5
AZM 10
AZM 50
p62/SQSTM1
Control
AZM-N Ox 2.5
AZM-N Ox 10
AZM-N Ox 50
AZM 2.5
AZM 10
AZM 50
LC3B-II
Control
AZM-N Ox 2.5
AZM-N Ox 10
AZM-N Ox 50
AZM 2.5
AZM 10
AZM 50
1
10
100
Relative expression (log scale)
C
CONT
AZM-N-Ox 2.5
AZM-N-Ox 10
AZM-N-Ox 50
AZM 2.5
AZM 10
AZM 50
PARP
PARP CL
p62/SQSTM1
LC3B-I/II
Actin-β
116
89
62
14
16
45

Fig. 5

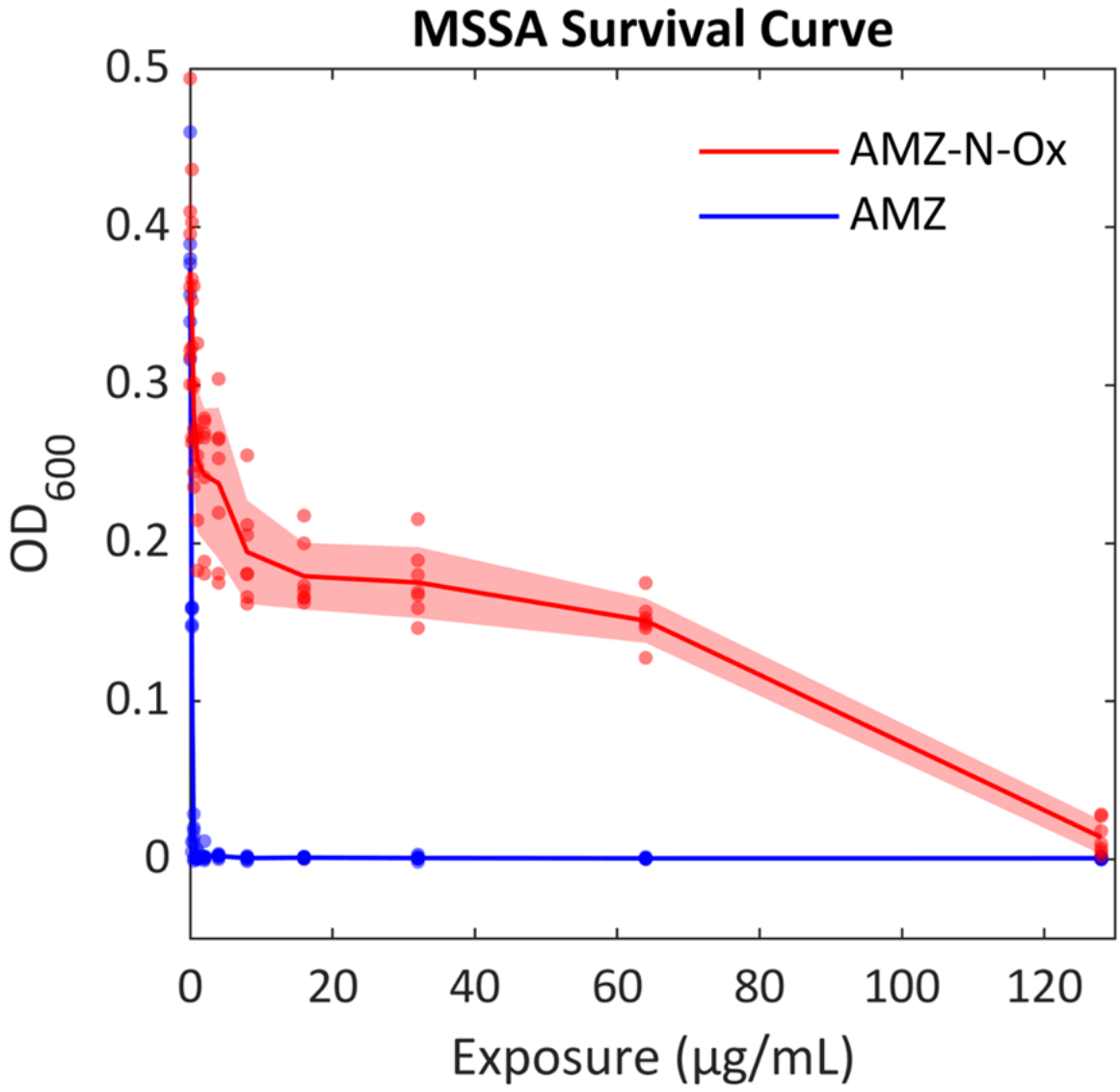
MSSA Survival Curve
AMZ-N-Ox
AMZ
OD600
0.5
0.4
0.3
0.2
0.1
0
0
20
40
60
80
100
120
Exposure (µg/mL)

Fig. 6

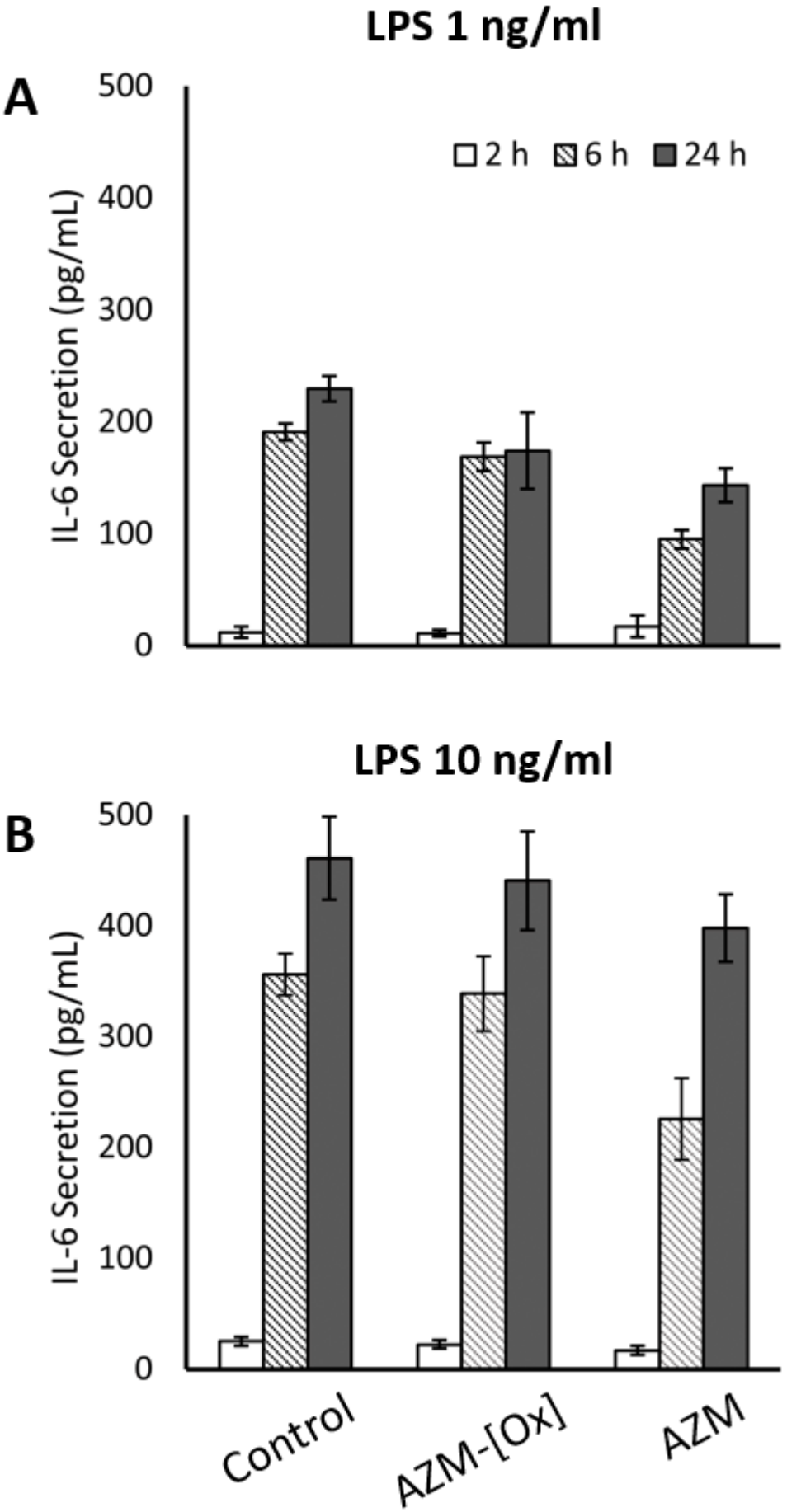
LPS 1 ng/ml
A
500
400
300
200
100
0
IL-6 Secretion (pg/mL)
2 h
6 h
24 h
LPS 10 ng/ml
B
500
400
300
200
100
0
IL-6 Secretion (pg/mL)
Control
AZM-[Ox]
AZM